A theoretical study of ethylene, cyclopentene and 1-amino-3-cyclopentene adsorption on the silicon $< 100 >$ surface

2006 J. Phys.: Condens. Matter 18 2349

(http://iopscience.iop.org/0953-8984/18/8/001)

INSTITUTE OF PHYSICS PUBLISHING JOURNAL OF PHYSICS: CONDENSED MATTER

J. Phys.: Condens. Matter **18** (2006) 2349–2365 doi:10.1088/0953-8984/18/8/001

A theoretical study of ethylene, cyclopentene and 1-amino-3-cyclopentene adsorption on the silicon ⟨100⟩ surface

G Cantele[1,3], F Trani[1], D Ninno[1], M Cossi[2] and V Barone[2]

[1] Coherentia CNR-INFM and Università di Napoli 'Federico II', Dipartimento di Scienze Fisiche, Complesso Universitario M.S. Angelo, Via Cintia, I-80126 Napoli, Italy
[2] Università di Napoli 'Federico II', Dipartimento di Chimica, Complesso Universitario M.S. Angelo, Via Cintia, I-80126 Napoli, Italy

E-mail: Giovanni.Cantele@na.infn.it

Received 26 September 2005, in final form 22 December 2005
Published 10 February 2006
Online at stacks.iop.org/JPhysCM/18/2349

Abstract

In this paper we report on a comparative *ab initio* study of the adsorption of ethylene, cyclopentene and 1-amino-3-cyclopentene on the silicon ⟨100⟩ surface. Accurate calculations of the reaction path have been carried out using a cluster model for the surface dimer (Si_9H_{12}) and Gaussian-type basis functions. The dependence of the computed reaction path on the theoretical method is investigated; activation energies turn out to be quite independent of the method, and general trends can be found for the three systems studied: the larger difference is found between linear and cyclic alkenes. Periodic calculations with plane waves are also performed on periodic slabs, finding an adsorption energy in fair agreement with the cluster model. The surface band structure is carefully studied: a strong dispersion is found along some directions for highly covered surfaces, in good agreement with the experimental data available for ethylene. Also in this case, differences arise when passing from linear to cyclic alkenes, while the second substituent on the cycle has very limited effects.

(Some figures in this article are in colour only in the electronic version)

1. Introduction

The interest in the functionalization of semiconductor surfaces has grown more and more in recent years [1–5]. Interfacing semiconductor systems with biological and chemical species presents many technological interests. The controlled coverage of surfaces with organic molecules is the challenging route toward the fabrication of new devices, with applications ranging from medicine and biology (sensing devices for drugs, viruses, proteins, etc) to

[3] Author to whom any correspondence should be addressed.

molecular electronics. In all these fields exciting new opportunities are offered by nanosized semiconductors, which are ideal for biological labelling due to their size-tunable light emission coupled to dimensions comparable to those of the species to be sensed [6].

One of the most investigated surfaces is the silicon ⟨100⟩ surface whose high chemical reactivity is well known [3–5]. Most of the peculiar characteristics of this surface are related to the formation of Si–Si dimers, as a result of the surface reconstruction. At variance with the analogous diamond surface, such silicon dimers show geometrical buckling, which results in nonequivalent surface Si atoms, with the consequent charge transfer from the down Si atom to its upper counterpart. Such an asymmetry is responsible for the enhanced chemical reactivity of the surface. Indeed, it has been argued that the chemisorption of an organic molecule containing a C=C double bond can occur via a process known as a $[2+2]$ cycloaddition. Both this bond and the Si–Si bond within a dimer break, with the formation of two C–Si σ-type bonds. It is well known that $[2+2]$ cycloaddition would be thermally forbidden for symmetric surface dimers [3]. Instead, for the reconstructed silicon ⟨100⟩ surface the reaction occurs with relatively low energy barriers, giving rise to stable covered surfaces, suitable for further studies and chemical reactions. Thus, the silicon ⟨100⟩ surface provides the route to realizing desired coverages via direct C–Si bonds and the consequent fabrication of stable and reproducible substrates, which can be easily integrated in current microelectronics technologies.

Controlled coverage has been obtained for a huge number of molecules, among which we cite C_2H_4 [7–9] and C_5H_8 [10–12], but many other examples could be given [1–5]. In many cases the coverage is viewed only as an intermediate step, known as surface functionalization. One of the most relevant examples is sequential DNA attaching, made possible if the coverage is realized via 'double-face' molecules, namely, molecules which possess a double C=C bond for anchoring to the surface and another functional group (e.g. an amine group) which can act as a cross-linker to DNA [13, 14].

Of course, understanding the chemical pathways which control the interaction between the surface and the C=C bond is crucial for the fine tuning of surface functionalization. Although several aspects have been elucidated in recent years, quantum mechanical (QM) computations can offer further insight provided that the due attention is devoted to the selection of both the computational and the material models. We have thus initiated a comprehensive research programme on this subject, by means of methods rooted in density functional theory (DFT). In a previous paper, we have analysed the selection of proper cluster models and the possibility of integrating the results of localized (Gaussian) and delocalized (plane-wave) basis sets [15]. Here we present a comparative study of the adsorption of ethylene (C_2H_4), cyclopentene (C_5H_8) and 1-amino-3-cyclopentene ($C_5H_7NH_2$) with the aim of obtaining further insights into the changes in reactivity and electronic properties passing from linear alkenes to five-membered rings (C_2H_4 versus C_5H_8 and $C_5H_7NH_2$), and when an amino group is introduced (C_5H_8 versus $C_5H_7NH_2$). In view of our previous results, the reaction path leading to the adsorption of the three molecules on the silicon ⟨100⟩ surface is studied on Si_9H_{12}-molecule complexes using a localized basis set (Gaussian orbitals, GOs). Comparing our results to those obtained in previous computations, performed by both localized and delocalized basis sets [17–21, 23–27, 29, 31–33], we show that the chemisorption energies are quite sensitive to the choice of the functional and the model cluster, whereas activation energies are more stable. On the other hand, a clear trend is found on passing from the linear to the cyclic alkenes, while the amino group has a limited influence on the reaction path. Because, in contrast to the case of isolated adsorbates on nanocrystals, most of the experiments have been done on extended surfaces with high coverage, it can be interesting to compare the adsorbate–surface complex properties using periodically repeated slabs as a model. Plane-wave (PW) calculations in the presence of the three molecules and for different coverages are performed and the adsorption

energies calculated. A comparison is done with the results obtained using GOs. Moreover, the surface electronic properties are analysed, using weighted band structure and projected density of states plots. This allows us to bring out adsorbate-related features of the band structure and to distinguish between the three adsorbates. In the case of C_2H_4 we show that a fair agreement is found with angle-resolved electron photoemission spectroscopy experiments on fully covered silicon surfaces.

2. The method

All the calculations have been performed in the framework of density functional theory. The complete characterization of the reaction path for the adsorption of the three cited molecules has been done using the Gaussian03 package [34], and the Si_9H_{12} cluster, whose reliability has been discussed in [15]. The optimized geometries (reactants, products, intermediate and transition states along the reaction path) have been found by allowing the full relaxation of all the atoms. For these optimizations we used the PBE1PBE density functional (also known as PBE0) [35], which corrects the Perdew–Burke–Ernzerhof (PBE) [36] functional by a predefined fraction (1/4) of Hartree–Fock exchange (it belongs to the family of hybrid functionals [37, 38] that have proved to be more reliable than their conventional counterparts for the calculation of bond structures and energies). A mixed basis set was used consisting of the LANL2DZ effective core potentials (ECPs) and related basis set [39] for all the atoms of the Si_9H_{12} cluster but the two Si atoms of the dimer. For these atoms and all those of the organic molecule we used the all-electron 6-31G(d, p) basis set [40], including polarization functions on all the atoms. Using geometries optimized at this level, we computed the adsorption energy and the activation barrier with a variety of functionals (PBE, PBE1PBE, B3LYP [41]), to compare our results with previous findings and account for the spread in the results documented in the literature.

The reaction path calculations were performed by identifying the minima and the corresponding saddle points on the potential surface and computing the intrinsic reaction coordinate (IRC) around the saddle point; the nature of the stationary points was confirmed by computing the energy second derivatives with respect to nuclear motions. The curves were then completed with minimizations ending to reactants and products. All the stationary points were characterized by computing the energy second derivatives, which also allowed the calculation of the temperature dependent vibrational contributions to the free energy in the framework of the harmonic oscillator/rigid rotor model. The basis set superposition error (BSSE) [42], causing the overestimation of the adsorption energies due to the larger set of basis functions available in the complex than in the separate reagents, was corrected by the counterpoise method, i.e. computing both reagent energies in the presence of the basis functions of the partner.

The electronic properties of the extended surface have been characterized within a periodic slab model using a plane-wave-based approach, implemented in the Quantum-ESPRESSO package [43], within the GGA-PBE approximation. We used ultrasoft pseudopotentials to describe the C, H, and N atoms and norm-conserving pseudopotential for the Si atom. The cut-off for the plane-wave basis set was fixed to 30 Ryd, which gives quite converged results on the adsorption energies and relaxed geometries. Vacuum space equivalent to 6 Si atomic layers separated periodic replicas of the slab. No significant modification of all the calculated properties was found on increasing the vacuum space. Each slab is constituted by 12 Si atomic layers, with the two central ones kept fixed during all the relaxations and adsorbed molecules on both sides of the slab itself. Some further details about the calculation can be found in [15]. The reconstructed clean silicon surface was optimized using a 2×2 surface unit cell, corresponding to alternatively buckled dimers along the dimer rows. C_2H_4-, C_5H_8- and $C_5H_7NH_2$-covered

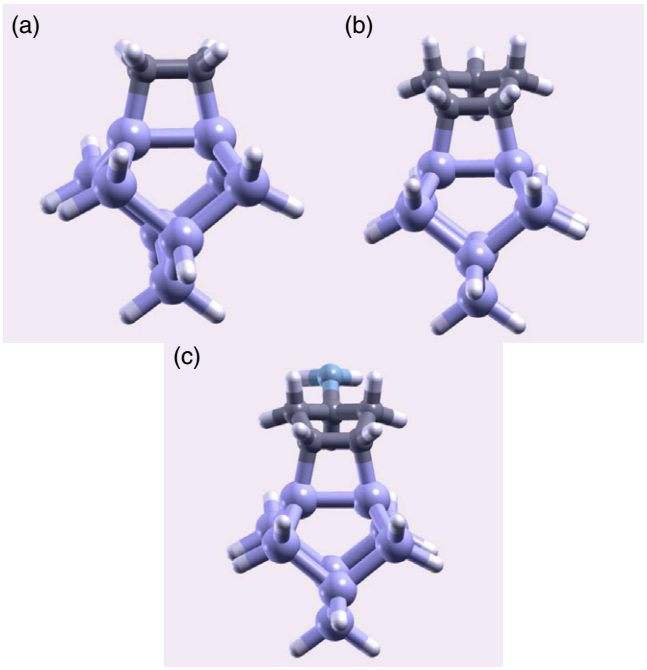

Figure 1. The structures of the three Si_9H_{12}-molecule complexes: (a) ethylene, (b) cyclopentene, (c) 1-amino-3-cyclopentene.

surfaces were studied using both 2×1 and 2×2 surface unit cells, to model fully covered (1.0 monolayer, one adsorbed molecule per dimer) and half covered (0.5 monolayer, one adsorbed molecule per dimer pair) surfaces respectively. The Brillouin zones of the 2×1 and 2×2 surface unit cells were sampled using $2 \times 4 \times 1$ and $2 \times 2 \times 1$ Monkhorst–Pack meshes respectively.

It is worth mentioning that to compare the different band structures coming from the clean and covered surfaces, an alignment procedure of the band energies is needed. For this purpose, the self-consistent electrostatic potential was calculated for all the considered systems (clean surface with 2×2 reconstruction and covered surface with C_2H_4, C_5H_8 and $C_5H_7NH_2$); the same potential can be calculated for bulk silicon (with the same surface supercell, after removing the empty space). A planar average (on planes parallel to the surface) of the potential was then performed: the oscillating profile of the averaged potential for all the systems follows that of the bulk silicon in the central layer, where a bulk-like behaviour is expected. The potential alignment was obtained by requiring that in the two central layers the mean value is the same as for bulk silicon. The same shifts were then applied to the corresponding band structures, retrieving an almost perfect alignment (e.g. deep energy levels, present in all the systems and which are not affected by the molecule–surface interaction, show complete overlap).

3. Results

3.1. The reaction path

The reaction path for the adsorption of the three organic molecules on the Si_9H_{12} cluster was completely characterized using GOs (the hybrid density functional PBE1PBE was used in all the optimizations): the optimized Si_9H_{12}-molecule complexes are shown in figure 1. A

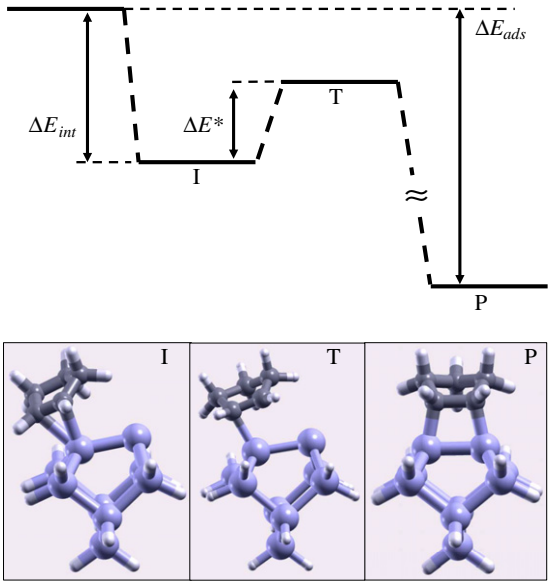

Figure 2. A schematic drawing of the reaction path for the adsorption of the three organic molecules on the Si_9H_{12} cluster. The geometries for the intermediate state (I), the transition state (T) and the products (P) are referred to the C_5H_8–Si_9H_{12} complex.

Table 1. Reaction path for C_2H_4 calculated with different methods (results with counterpoise correction to BSSE in parentheses, all values in kcal mol^{-1}, geometries optimized at PBE1PBE level); $\Delta E_{\rm int} = E_{\rm intermediate} - E_{\rm reactants}$, $\Delta E_{\rm ads} = E_{\rm product} - E_{\rm reactants}$, $\Delta E^* = E_{\rm TS} - E_{\rm intermediate}$.

	PBE1PBE	B3LYP	PBE	BLYP	MP2
$\Delta E_{\rm int}$	−13.6 (−10.3)	−5.6 (−2.2)	−12.4 (−8.9)	−3.1 (0.5)	−4.4
$\Delta E_{\rm ads}$	−61.1 (−57.0)	−50.5 (−46.0)	−54.3 (−50.0)	−43.0 (−38.2)	−56.1
ΔE^*	1.9 (2.1)	3.4 (3.5)	1.9 (2.0)	3.4 (3.6)	2.5

Table 2. Reaction path for C_5H_8 calculated with different methods (results with counterpoise correction to BSSE in parentheses, all values in kcal mol^{-1}, geometries optimized at PBE1PBE level, same symbols as in table 1).

	PBE1PBE	B3LYP	PBE	BLYP	MP2
$\Delta E_{\rm int}$	−16.8 (−12.9)	−6.3 (−2.5)	−13.9 (−10.1)	−2.1 (1.9)	−10.3
$\Delta E_{\rm ads}$	−55.0 (−50.1)	−42.6 (−37.3)	−47.4 (−42.3)	−34.1 (−28.4)	−54.9
ΔE^*	5.7 (5.8)	6.1 (6.5)	4.8 (5.2)	5.6 (6.2)	6.9

schematic drawing of the reaction path is illustrated in figure 2; the main energy differences describing the reaction are reported in tables 1, 2 and 3 for C_2H_4, C_5H_8 and $C_5H_7NH_2$ respectively. Here, $\Delta E_{\rm int}$ is the difference between the intermediate and the reactant energies, $\Delta E_{\rm ads}$ is the adsorption energy (i.e. the difference between the final product and the reactants), and $\Delta E^\star$ is the activation barrier, i.e. the difference between the transition state and the intermediate energies. In tables 1–3 we also report the energy differences computed with different density functionals at the same geometries.

From the chemical point of view, the most interesting observation is that for all three molecules the adsorption reaction proceeds through a very similar mechanism, based on an

Table 3. Reaction path for $C_5H_7NH_2$ calculated with different methods (results with counterpoise correction to BSSE in parentheses, all values in kcal mol^{-1}, geometries optimized at PBE1PBE level, same symbols as in table 1).

	PBE1PBE	B3LYP	PBE	BLYP	MP2
ΔE_{int}	−16.9 (−12.8)	−6.3 (−2.2)	−14.0 (−9.7)	−1.9 (2.5)	−9.5
ΔE_{ads}	−55.6 (−50.6)	−42.8 (−37.4)	−47.8 (−42.5)	−34.1 (−28.2)	−54.5
ΔE^*	5.6 (5.7)	6.2 (6.4)	4.9 (5.0)	5.7 (6.0)	6.9

Table 4. Reaction path energies (kcal mol^{-1}) for the three molecules on Si_9H_{12} computed with the PBE1PBE functional, including thermal contributions (zero-point, harmonic vibrational and rotational energies at 298 K), without BSSE corrections.

	C_2H_4	C_5H_8	$C_5H_7NH_2$
ΔE_{int}	−12.4	−15.2	−15.2
ΔE_{ads}	−59.7	−53.0	−53.5
ΔE^*	1.7	4.8	4.7

asymmetric intermediate and a zwitterionic transition state. First an intermediate state is reached, resulting from the nucleophilic attack of the incoming alkenic π-bond to the down-lying, electron-deficient Si atom of the surface dimer: the intermediate is formed from the separate reactants without any energy barrier. Then, an activated process leads to the final complex, in which the Si dimer is substituted by two Si–C bonds (and the two Si atoms become completely equivalent): the barrier for this step is computed in the range 1.9–3.4 kcal mol^{-1} for ethylene and 4.8–6.2 kcal mol^{-1} for the cyclic molecules. For all the systems the intermediate is quite stable with respect to the reactants and the overall reaction is strongly exothermic, though the actual values of ΔE_{int} and ΔE_{ads} are quite dependent on the calculation level (this point deserves a deeper analysis, and is considered below).

In table 4 we report the relevant reaction path energies with vibrational and rotational contributions at 298 K, computed with the PBE1PBE functional: these quantities should be compared with the ΔE values in the first columns of tables 1–3 to estimate the thermal corrections, which are likely to be much less dependent on the calculation level than the electronic energies. In general, such corrections are quite small, and they do not affect the shape of the reaction path for the systems considered here.

Interestingly, very similar results are obtained for C_5H_8 and $C_5H_7NH_2$. The reaction with C_2H_4 occurs with a larger adsorption energy and a smaller barrier, while the addition of the amine group to C_5H_8 does not significantly change the reaction path: the energetics of the Si–C bond formation is dominated by the local chemical environment (in particular by the slight distortion of the π system due to the cycle in C_5H_8 and $C_5H_7NH_2$). One can foresee that a similar reaction path will also be found for substituents other than the amino group, unless significant steric effects become operative with bulky groups.

As pointed out above, both ΔE_{int} and ΔE_{ads} show significant differences according to the exchange–correlation functional used, and this is consistent with the large spread of the results found in the literature. Previous findings, obtained using GOs as well as PWs, slab or cluster models, are summarized in tables 5 and 6 for C_2H_4 and C_5H_8 respectively; some of these results had also been collected in [29]. Reference [33] also reports an adsorption energy for $C_5H_7NH_2$ of −36.1 kcal mol^{-1} (−1.57 eV) calculated within a cluster model using GOs and a hybrid DFT-semiempirical method. In table 5 an experimental measurement of the adsorption energy is reported as well. The choice of the exchange–correlation functional appears to be

Table 5. Adsorption energies for C_2H_4 on silicon ⟨100⟩ surface from previous theoretical studies. One set of experimental data is reported as well. Some of these results are also summarized in [29]. PS stands for periodic slab.

Functional	Basis set	Model	ΔE_{ads} kcal mol^{-1} (eV)	Ref.
X_α		$Si_{20}H_{18}$ (symmetric dimer)	−70.6 (−3.06)	[16]
LDA	PAW	PS (4 × 2-0.25 ML)	−36.2 (−1.57)	[17]
LDA-PZ	PW	PS (2 × 1-1 ML)	−60.6 (−2.63)	[18]
GGA-PW91		PS (2 × 1-1 ML)	−41.7 (−1.81)	
B3LYP	6-31G*	Si_9H_{12}	−45.7 (−1.98)	[20]
	6-311G**		−43.2 (−1.87)	
GGA-PBE	PW	PS (2 × 1-1 ML)	−43.6 (−1.89)	[21]
		PS (2 × 2-0.5 ML)	−44.5 (−1.93)	
GGA-PBE	PW	PS (2 × 2-0.5 ML)	−48.4 (−2.10)	[22]
EDF1	6-31G*	Two-dimer cluster (0.5 ML)	−42.9 (−1.86)	[26]
	LANL2DZ		−42.7 (−1.85)	
B3LYP	6-31G*		−49.1 (−2.13)	
	LANL2DZ		−54.6 (−2.37)	
EDF1	6-31G*	Two-dimer cluster (1 ML)	−41.0 (−1.78)	
	LANL2DZ		−40.4 (−1.75)	
B3LYP	6-31G*		−47.7 (−2.07)	
	LANL2DZ		−53.0 (−2.30)	
EDF1	6-31G*	Si_9H_{12}	−40.4 (−1.75)	
	LANL2DZ		−40.1 (−1.74)	
B3LYP	6-31G*		−45.9 (−1.99)	
	LANL2DZ		−45.4 (−1.97)	
GGA-PBE	PW	PS (2 × 1-1 ML)	−44.0 (−1.91)	[27]
		PS (2 × 2-0.5 ML)	−44.7 (−1.94)	
GGA-PBE	PW	PS (2 × 4-0.25 ML)	−47.9 (−2.08)	[28]
B3LYP	cc-pVDZ	Si_9H_{12}	−51.1 (−2.22)	[29]
		$Si_{21}H_{20}$	−46.1 (−2.00)	
		$Si_{33}H_{28}$	−44.3 (−1.92)	
		$Si_{45}H_{36}$	−44.5 (−1.93)	
B3LYP	6-31G*	Si_9H_{12}	−40.7 (−1.77)	[31]
MP2	6-31G*		−42.2 (−1.83)	
MP2	6-31G(d)	$Si_{48}H_{40}$	−33.0 (−1.43)	[32]
		Experiment	−38.0 (−1.65)	[44]

crucial, since the results show variations within an interval of tens of kcal mol^{-1}, even if in some cases it is not clear if thermal corrections have been added to the potential energies. From our results, it is apparent that the same variations are obtained between PBE1PBE and B3LYP and between their conventional counterparts (PBE and BLYP, respectively; note that PBE is the current shorthand for PBEPBE). Thus the difference is not related to the amount of the Hartree–Fock exchange included in the method: a likely hypothesis is that the difference lies in the treatment of the correlation energy. This idea can be tested by repeating the calculation with the non-standard BPBE and PBELYP functionals (in the former the Becke exchange functional is coupled to the PBE correlation functional, while in the latter the PBE exchange is used with the Lee–Yang–Parr correlation). For the C_2H_4–Si_9H_{12} complex we found (the values corrected

Table 6. Calculated adsorption energies for C_5H_8 on the silicon ⟨100⟩ surface from previous studies. PS stands for periodic slab.

Functional	Basis set	Model	ΔE_{ads} kcal mol^{-1} (eV)	Ref.
GGA-PBE	PW	PS (2 × 2-0.5 ML-*cis*)	−34.8 (−1.51)	[23]
		PS (2 × 2-0.5 ML-*trans*)	−27.9 (−1.21)	
		PS (2 × 2-1 ML-*cis*)	−21.7 (−0.94)	
		PS (2 × 2-1 ML-*trans*)	−24.2 (−1.05)	
GGA-PBE	PW	PS (2 × 2-0.5 ML-*cis*)	−36.9 (−1.60)	[24]
		PS (2 × 2-1 ML-*cis*)	−27.0 (−1.17)	
LDA-PZ	PW	PS (2 × 2-1 ML-*cis*)	−32.3 (−1.40)	[25]
		PS (2 × 2-1 ML-*trans*)	−36.9 (−1.60)	
GGA-PBE		PS (2 × 2-1 ML-*cis*)	−13.8 (−0.60)	
		PS (2 × 2-1 ML-*trans*)	−18.4 (−0.80)	
GGA	PW	PS (2 × 2-0.5 ML)	−35.0 (−1.52)	[30]
		PS (2 × 2-1 ML)	−28.0 (−1.21)	
B3LYP + AM1	6-311 + G/AM1	$Si_{197}H_{108}$ (*cis*)	−36.4 (−1.58)	[33]

Table 7. Adsorption energies for fully (1 ML) and half (0.5 ML) covered surfaces calculated for periodically repeated slabs using plane waves. 2 × 1 and 2 × 2 surface unit cell are used for 1 ML and 0.5 ML respectively. For C_5H_8 the configuration shown here corresponds to the one mentioned as '*cis*' in table 6.

Adsorbate	Coverage (ML)	ΔE_{ads} kcal mol^{-1} (eV)
C_2H_4	1.0	−40.8 (−1.770)
	0.5	−41.4 (−1.795)
C_5H_8	1.0	−21.5 (−0.935)
	0.5	−35.1 (−1.522)
$C_5H_7NH_2$	1.0	−22.1 (−0.960)
	0.5	−35.6 (−1.545)

for the BSSE are in parentheses): $\Delta E_{int} = -8.9$ (−5.6) and −6.7 (−2.6) kcal mol^{-1}, and $\Delta E_{ads} = -50.9$ (−47.1) and −46.4 (−40.8) kcal mol^{-1} with BPBE and PBELYP, respectively.

Comparing these energies with the corresponding PBEPBE and BLYP values in table 1, we see that the correlation functional is actually responsible for most of the difference, though the exchange contribution is not completely negligible: on the other hand, the PBE1PBE and B3LYP results show that the Hartree–Fock exchange affects the Becke and the PBE functionals in a very similar way. This analysis sheds some light on the origin of the dependence of results on the computational model, but it remains still unclear what are the most reliable ΔE. The MP2 results reported in tables 1–3 are closer to B3LYP for ΔE_{int} and to PBE1PBE for ΔE_{ads} (in this last case the agreement is very good): note that the counterpoise corrected MP2 results are not reported because the BSSE is very large for MP2 unless very large basis sets are used, and the comparison would be less significant. It is worth noting that the reaction barriers are much less dependent on the computational model.

In summary, even if the DFT calculations cannot provide a safe value for the reaction free energies, they clearly show that the greatest differences in the reaction path energetics appear when passing from linear to cyclic molecules (that is, when the C=C double bond is distorted), and that the presence of the amino group on the cycle has a very limited effect on the adsorption kinetics and thermodynamics.

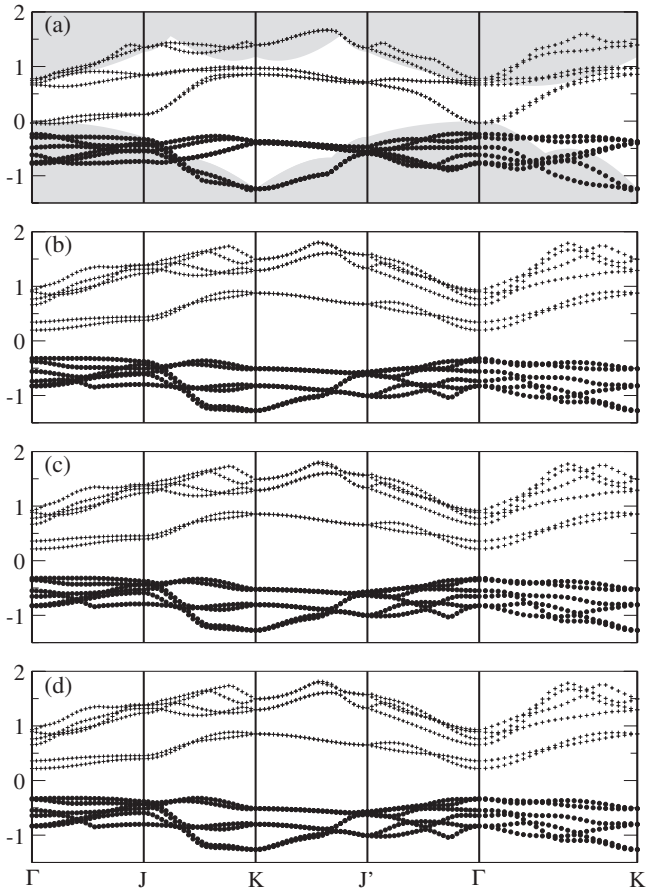

Figure 3. Surface band structure for (a) clean, (b) C_2H_4-, (c) C_5H_8- and (d) $C_5H_7NH_2$-covered silicon ⟨100⟩ surface (0.5 ML). All the band structures are calculated using a 2×2 surface unit cell. The notation for Γ, J, J′ and K points is the same as in [45]. The shaded area in (a) is a projection of the bulk silicon band structure within the surface Brillouin zone. The reference energy is the top valence band of bulk silicon. Bold circles and crosses correspond to occupied and unoccupied bands respectively.

3.2. Adsorption on extended surfaces

Most of the available experiments on silicon covered surfaces concern macroscopic surfaces. Both experimental and theoretical studies of the surface electronic band structure are not very numerous in the literature [19]. For example, recent angle-resolved photoelectron spectroscopy experiments [9, 19] revealed the presence of one-dimensional delocalized adsorbate Bloch states for a fully covered C_2H_4–silicon ⟨100⟩ surface. They also gave insight into direct adsorbate–adsorbate interaction along the dimer rows and showed fair agreement with the *ab initio* theoretical predictions. Therefore, it can be interesting to compare such adsorbate-related features of the band structure for different adsorbates as well as for different surface coverages. In this section we show the results of plane-wave-based calculations performed on periodically repeated slabs. Both fully and half covered (1.0 and 0.5 monolayer (ML) respectively) surfaces were considered, and the adsorption energies were estimated from total energy calculations. Such energies can be compared with those shown in the previous section

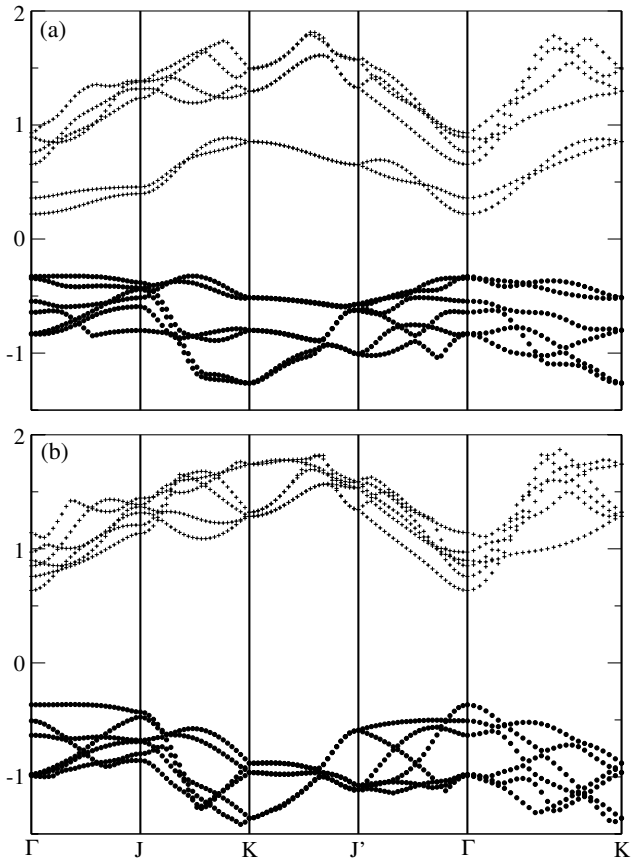

Figure 4. Surface band structure for the $C_5H_7NH_2$-covered silicon ⟨100⟩ surface with (a) 0.5 ML and (b) 1.0 ML coverage. In both cases a 2×2 surface unit cell is considered. The notation for Γ, J, J′ and K points is the same as in [45]. The reference energy is the top valence band of bulk silicon. Bold circles and crosses correspond to occupied and unoccupied bands respectively.

for the cluster model treated using localized atomic orbitals. A summary for such energies is reported in table 7. It is worth mentioning that on increasing the cut-off up to 40 Ryd just a few meV variations on the adsorption energies were found, while the results are converged within less then 0.1 eV with respect to the *k*-point grid (for example, the adsorption energy for the $C_5H_7NH_2$ adsorbate with a 0.5 ML coverage and a $4 \times 4 \times 1$ grid is -1.622 eV, to be compared with -1.545 eV in table 7).

First, we point out that fair agreement is found with previous results present in the literature for plane wave calculations (see tables 5 and 6). The lower coverage appears to be more stable, for all three considered adsorbates, due to a weaker interaction of hydrogens belonging to neighbour molecules. Moreover, adsorption of ethylene appears to be favoured over C_5H_8 and $C_5H_7NH_2$ adsorption, and these last two show very similar adsorption energies.

The comparison with the adsorption energies shown in the previous section is more difficult, because the periodic model includes adsorbate–adsorbate interactions which are absent in the cluster model analysed using localized atomic orbitals. Nevertheless, we can see that if we consider our results for a 0.5 ML coverage (for which interactions are lower) the general trend is in agreement with the results of the previous section. The adsorption energy

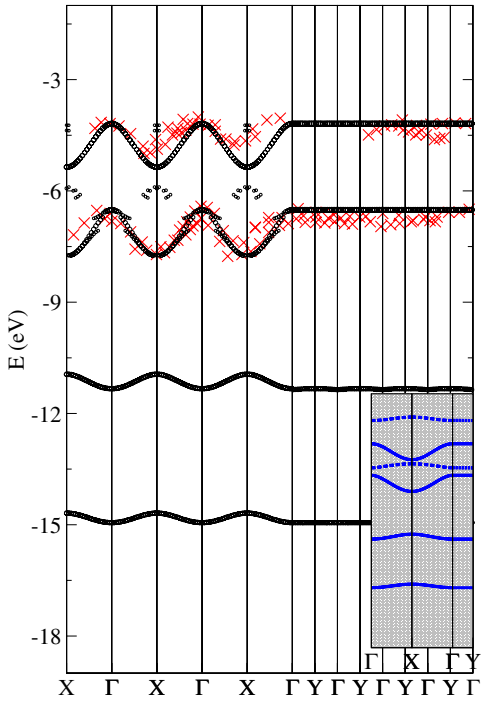

Figure 5. The weighted band structure for C_2H_4 adsorbed on the silicon ⟨100⟩ surface with a 1.0 ML coverage. The surface band structure is calculated using a 2×1 surface unit cell along the X–Γ and Γ–Y lines (the k_x direction being parallel to the dimer rows), and repeated outside the first Brillouin zone. The size of each point is proportional to the projection of the corresponding electronic state on the adsorbate atomic orbitals. The crosses are experimental data from [9], after a rigid shift. The inset shows the same band structure obtained after removal of all the silicon atoms from the surface unit cell. The zero energy corresponds to the top valence band of bulk silicon.

of C_2H_4 is 6.3 kcal mol^{-1} more negative than that of C_5H_8 and 5.5 kcal mol^{-1} more negative than that of $C_5H_7NH_2$. The same differences, obtained from tables 1, 2 and 3 (the PBE column should be considered, being the plane-waves results obtained within GGA-PBE), are 7.7 and 7.5 kcal mol^{-1}, which can be considered to be in satisfactory agreement.

Further considerations can be drawn, as previously discussed, looking at the surface band structures and the associated density of states. The band structures have been aligned by requiring the averaged electrostatic potential within the slab core to be the same as bulk silicon (see section 2). In all the results that follow, we assume as zero energy the top valence band of bulk silicon.

The highest occupied and lowest unoccupied bands are shown in figure 3, where we compare the results obtained for the clean Si surface (with a 2×2 reconstruction, showing alternatively buckled dimers along the dimer rows), and the C_2H_4-, C_5H_8-, and $C_5H_7NH_2$-covered surfaces ((a) to (d) respectively). The surface coverage is 0.5 ML, corresponding to one adsorbed molecule per dimer pair. The presence of the adsorbed molecule is shown to partially remove the surface states (related to the Si–Si dimers) lying within the bulk silicon energy gap. The remaining surface states (just above 0 eV, at Γ point) are those related to the unsaturated silicon dimers. This is also confirmed by comparing 0.5 and 1.0 ML covered surfaces, as shown in figure 4 for the $C_5H_7NH_2$ adsorbate. In the second case, all the intra-gap states disappear, corresponding to the formation of two C–Si σ bonds at each dimer site.

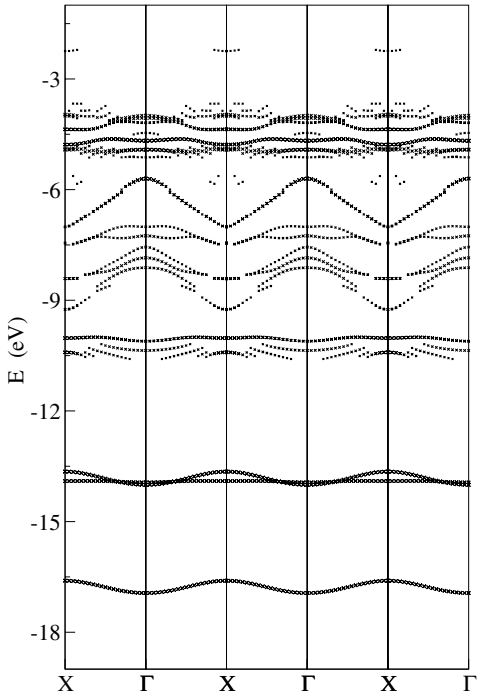

Figure 6. The weighted band structure for C_5H_8 adsorbed on the silicon ⟨100⟩ surface with a 1.0 ML coverage. The surface band structure is calculated using a 2×1 surface unit cell along the X–Γ line (the k_x direction being parallel to the dimer rows), and repeated outside the first Brillouin zone. The size of each point is proportional to the projection of the corresponding electronic state on the adsorbate atomic orbitals. The zero energy corresponds to the top valence band of bulk silicon.

The comparison of the band structures in figure 3 shows that no significant features of the band structure strongly related to the adsorbate species are found as far as near-gap electronic levels are concerned. Some adsorbate-related bands can be found at lower energies and can be clearly identified looking at weighted band structure plots. To compare our results with the experiments of [9], we consider fully covered surfaces (1.0 ML, 2×1 surface unit cell). Starting from the projected density of states, we plot the band structure along the X–Γ line (parallel to the dimer rows), by giving to each point a size which is proportional to the projection of the corresponding wavefunction onto the adsorbate atomic orbitals. The results are shown in figures 5, 6 and 7 for C_2H_4, C_5H_8 and $C_5H_7NH_2$ respectively. For C_2H_4, the band structure along the Γ–Y line (orthogonal to the dimer rows) is shown as well. The energy bands are periodically repeated outside the first Brillouin zone, to more clearly bring out the levels that have dispersion. Electronic levels with a less than 50% projection have been skipped.

In the case of C_2H_4 we also report the experimental angle-resolved photoelectron spectroscopy results of [9] (figure 5, crosses), which have been rigidly shifted. A fair agreement with the experiments is shown, as was also found in [9, 19], confirming the reliability of our description of the surface electronic structure, and the plausibility of the analogous spectra computed for C_5H_8 and $C_5H_7NH_2$. Four main adsorbate-related bands are found. The two lowest-lying ones appear to be almost flat, corresponding to strongly localized levels. The two upper ones, instead, show significant dispersion along the X–Γ direction (of 1.22 and 1.18 eV respectively, to be compared with the experimental values 1.2 and 0.8 eV), while being

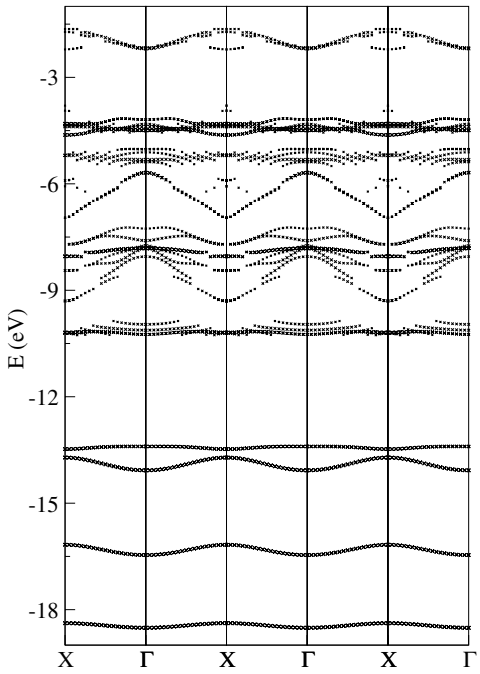

Figure 7. The weighted band structure for $C_5H_7NH_2$ adsorbed on the silicon ⟨100⟩ surface with a 1.0 ML coverage. The surface band structure is calculated using a 2×1 surface unit cell along the X–Γ line (the k_x direction being parallel to the dimer rows), and repeated outside the first Brillouin zone. The size of each point is proportional to the projection of the corresponding electronic state on the adsorbate atomic orbitals. The zero energy corresponds to the top valence band of bulk silicon.

completely flat in the Γ–Y direction. This is the signature of a strong adsorbate–adsorbate interaction along the dimer rows, which the experiment of [9] clearly showed. No significant interaction is found orthogonally to the dimer rows. Thus, it can be concluded that the surface Bloch states corresponding to these bands are one-dimensional, being extended only along the dimer rows.

The inset in figure 5 represents the energy bands along the X–Γ and Γ–Y lines for a fictitious system made of an isolated layer of C_2H_4 molecules obtained by just removing from the covered surface unit cell all silicon atoms. The solid lines correspond to the four adsorbate-related bands of the covered surface. It is remarkable that the dispersion of the two energy bands discussed above keeps unchanged, giving evidence for the fact that it is related to the interaction between adsorbate molecules, rather than to the underlying silicon surface.

A similar analysis can be carried out for C_5H_8 and $C_5H_7NH_2$ (figures 6 and 7). Even if we get in this case a more complicated picture (due to the higher number of adsorbate atomic orbitals), two main dispersed bands can be identified as for C_2H_4, but lying at lower energies. The comparison of C_5H_8 and $C_5H_7NH_2$ shows very similar features of this weighted band structure. It should be pointed out that the band structure along the Γ–Y line (not shown in the figures) even in this case has an almost dispersionless behaviour. We can conclude that experiments such as the one of [9] would distinguish between adsorbates made of linear and cyclic molecules containing a C=C double bond.

As a final step, we show, in figures 8 and 9 the projected density of states for the 1.0 and 0.5 ML coverages respectively. The projection is done onto the atomic orbitals of the adsorbate

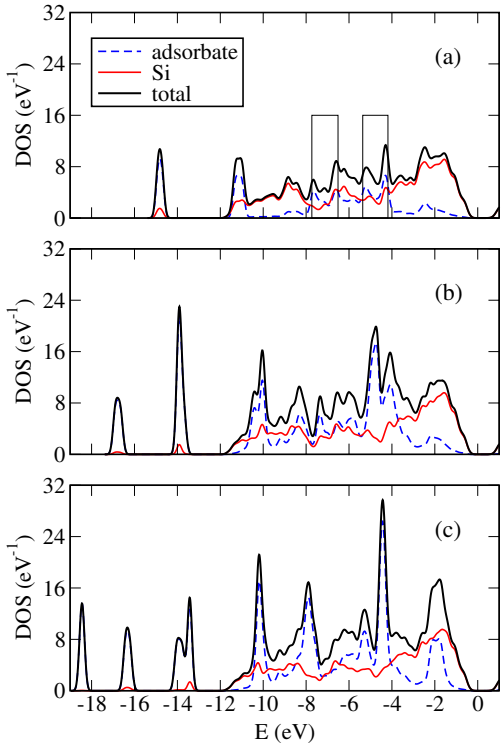

Figure 8. The density of states for a 1.0 ML coverage of (a) C_2H_4, (b) C_5H_8 and (c) $C_5H_7NH_2$ adsorbed on the silicon ⟨100⟩ surface, projected on the atomic orbitals of the adsorbate (thin dashed line) and of the first three silicon atomic layers (thin solid line). The thick solid line is the sum of the two previous ones. The two boxes identify the energy range spanned by the two dispersed bands of figure 5.

and of the surface and sub-surface silicon atoms (including the dimer rows and two silicon atomic layers below). In all these plots we report the separated contribution of the adsorbate (thin dashed line) and of the silicon surface (this solid line) as well as the sum of the two (thick solid line). The density of states for the clean 2×2-reconstructed silicon ⟨100⟩ surface is shown in figure 10 for comparison. In the case of C_2H_4 with a 1.0 ML coverage (figure 8(a)) we also show two boxes, indicating the energy range spanned by the two dispersed bands of figure 5. All these plots confirm the previous results. In particular, it is seen that near-gap energy states are mainly related to the silicon surface (thin solid lines are almost overlapped with the thick solid ones), and that no surface states are found for full surface coverage (band gap opening). Moreover, the adsorbate-related electronic levels (dashed lines) give rise to sharp peaks in the density of states for the half-covered surfaces, but to much more broadened bands for the fully covered surfaces, as a further confirmation that in the last case the interaction along the dimer rows is responsible for energy-dispersed electronic levels.

4. Conclusions

The present work is devoted to a comparative study of the adsorption of C_2H_4, C_5H_8 and $C_5H_7NH_2$ on the silicon ⟨100⟩ surface. First, we have fully characterized the reaction path for the three adsorbates, using a cluster model and localized orbital basis sets. All the molecule–

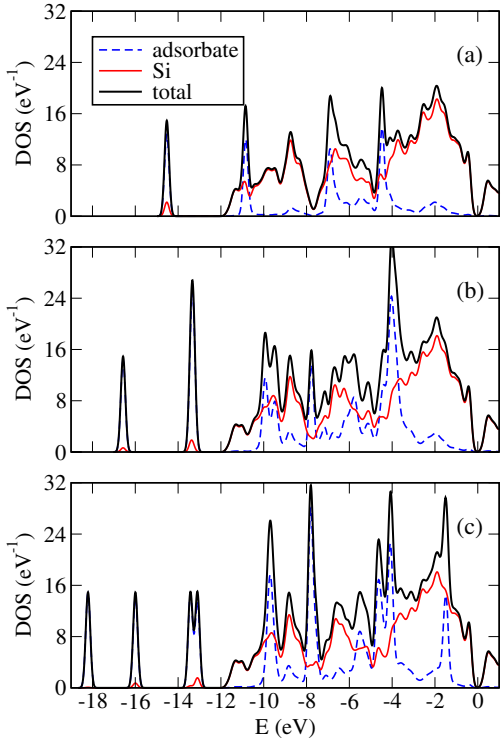

Figure 9. The density of states for a 0.5 ML coverage of (a) C_2H_4, (b) C_5H_8 and (c) $C_5H_7NH_2$ adsorbed on the silicon ⟨100⟩ surface, projected on the atomic orbitals of the adsorbate (thin dashed line) and of the first three silicon atomic layers (thin solid line). The thick solid line is the sum of the two previous ones.

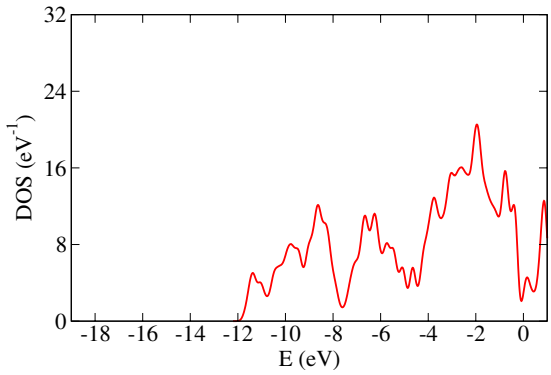

Figure 10. The density of states for the clean 2 × 2-reconstructed silicon ⟨100⟩ surface.

Si_9H_{12} complexes show similar reaction paths: the reaction and activation energies change significantly from ethylene to cyclopentene (due to the C=C double bond local distortion in the cycle), but are practically unaffected by the presence of the second substituent (the amino group) on the alkenic cycle. On this basis, one can foresee that also other substituted cyclopentenes (like those that have been proposed for a number of photoelectronic and

sensor applications) would present a similar behaviour, provided that steric effects are not predominant. The adsorption energies calculated for periodically repeated slabs are in fair agreement with results of previous calculations, and predict similar trends to those obtained within the cluster model. The present results, along with the large amount of literature data, show that the choice of the exchange–correlation functional can be critical for the quantitative estimate of the reaction energies: we have shown that most of the uncertainty derives from the correlation functional, even if the exchange contribution is not negligible.

The electronic structure of the periodic slab has been characterized as well. Using weighted band structure plots and projected density of states, we show that adsorbate-related electronic levels give rise, for the fully covered surface, to bands with a significant dispersion, which can be attributed to the adsorbate–adsorbate interaction along the dimer rows. Such interaction almost disappears for the half-covered surfaces, resulting in much sharper peaks in the density of states. The near-gap energy levels appear to be almost independent of the adsorbed molecular species.

Acknowledgments

Financial support from the projects INFM-PON-SVISENARIA, ENEA-POSSENTE, POR-CAMPANIA, and INSTM-PRISMA is acknowledged. All the calculations have been performed at 'Campus Computational Grid'-Università di Napoli 'Federico II' advanced computing facilities.

References

[1] Hamers R J and Wang Y 1996 *Chem. Rev.* **96** 1261 and references therein
[2] Wolkow R A 1999 *Annu. Rev. Chem.* **50** 413 and references therein
[3] Bent S F 2002 *Surf. Sci.* **500** 879 and references therein
[4] Filler M A and Bent S F 2003 *Prog. Surf. Sci.* **73** 1 and references therein
[5] Yoshinobu J 2004 *Prog. Surf. Sci.* **77** 37 and references therein
[6] Patolsky F and Lieber C M 2005 *Mater. Today* **8** 20
[7] Yoshinobu J, Tsuda H, Onchi M and Nishijima M 1987 *J. Chem. Phys.* **87** 7332
[8] Liu H and Hamers R J 1997 *J. Am. Chem. Soc.* **119** 7593
[9] Widdra W, Fink A, Gokhale S, Trischberger P and Menzel D 1998 *Phys. Rev. Lett.* **80** 4269
[10] Hamers R J, Hovis J S, Lee S, Liu H and Shan J 1997 *J. Phys. Chem.* B **101** 1489
[11] Hovis J S, Liu H and Hamers R J 1998 *Surf. Sci.* **402–404** 1
[12] Liu H and Hamers R J 1998 *Surf. Sci.* **416** 354
[13] Strother T, Hamers R J and Smith L M 2000 *Nucl. Acids Res.* **28** 3535
[14] Lin Z, Strother T, Cai W, Cao X, Smith L M and Hamers R J 2002 *Langmuir* **18** 78
[15] Festa G, Cossi M, Barone V, Cantele G, Ninno D and Iadonisi G 2005 *J. Chem. Phys.* **122** 184714
[16] Feng K, Liu Z H and Lin Z 1995 *Surf. Sci.* **329** 77
[17] Fisher A J, Blöchl P E and Briggs G A D 1997 *Surf. Sci.* **374** 298
[18] Pan W, Zhu T and Yang W 1997 *J. Chem. Phys.* **107** 3981
[19] Birkenheuer U, Gutdeutsch U, Tösch N, Fink A, Gokhale S, Menzel D, Trischberger P and Widdra W 1998 *J. Chem. Phys.* **108** 9868
[20] Koneĉný R and Doren D J 1998 *Surf. Sci.* **417** 169
[21] Cho J H, Kleinman L, Chan C T and Kim K S 2001 *Phys. Rev.* B **63** 073306
[22] Miotto R, Ferraz A C and Srivastava G P 2002 *Surf. Sci.* **507–510** 12
[23] Akagi K and Tsuneyuki S 2001 *Surf. Sci.* **493** 131
[24] Cho J H and Kleinman L 2001 *Phys. Rev.* B **64** 235420
[25] Lu W, Schmidt W G and Bernholc J 2003 *Phys. Rev.* B **68** 115327
[26] Phillips M A, Besley N A, Gill P M W and Moriarty P 2003 *Phys. Rev.* B **67** 035309
[27] Cho J H and Kleinman L 2004 *Phys. Rev.* B **69** 075303

[28] Nagao M, Umeyama H, Mukai K, Yamashita Y, Yoshinobu J, Akagi K and Tsuneyuki S 2004 *J. Am. Chem. Soc.* **126** 9922
[29] Nakai H, Katouda M and Kawamura Y 2004 *J. Chem. Phys.* **121** 4893
[30] Ferraz A C and Miotto R 2004 *Surf. Sci.* **566–568** 713
[31] Wang Y, Ma J, Inagaki S and Pei Y 2005 *J. Phys. Chem.* B **109** 5199
[32] Lee H S, Choi C H and Gordon M S 2005 *J. Phys. Chem.* B **109** 5067
[33] Santos H R R, Ramos M J and Gomes J A N F 2005 *Phys. Rev.* B **72** 075445
[34] Frisch M J *et al* 2003 *Gaussian03, release C.02* (Pittsburgh, PA: Gaussian)
[35] Adamo C and Barone V 1999 *J. Chem. Phys.* **110** 6158
[36] Perdew J P, Burke K and Ernzerhof M 1996 *Phys. Rev. Lett.* **77** 3865
[37] Becke A D 1996 *J. Chem. Phys.* **104** 1040
[38] Perdew J P, Ernzerhof M and Burke K 1996 *J. Chem. Phys.* **105** 9982
[39] Hay P J and Wadt W R 1985 *J. Chem. Phys.* **82** 270
Wadt W R and Hay P J 1985 *J. Chem. Phys.* **82** 284
Hay P J and Wadt W R 1985 *J. Chem. Phys.* **82** 299
[40] Hariharan P C and Pople J A 1973 *Theor. Chim. Acta* **28** 213
[41] Becke A D 1988 *Phys. Rev.* B **38** 3098
[42] Boys S F and Bernardi F 1970 *Mol. Phys.* **19** 553
[43] Baroni S *et al* http://www.pwscf.org
[44] Clemen L, Wallace R M, Taylor P A, Dresser M J, Choyke W J, Weinberg W H and Jates J T Jr 1992 *Surf. Sci.* **268** 205
[45] Ramstad A, Brocks G and Kelly P J 1995 *Phys. Rev.* B **51** 14504